Improving Aircraft Noise Predictions ConsideringFan Rotational Speed

Merino Martinez, Roberto; Heblij, Sander; Bergmans, Dick H.T.; Snellen, Mirjam; Simons, Dick

DOI
10.2514/1.C034849

Publication date
2018

Document Version
Accepted author manuscript

Published in
Journal of Aircraft: devoted to aeronautical science and technology

Improving Aircraft Noise Predictions Considering the Fan Rotational Speed

Roberto Merino-Martínez[a]
Delft University of Technology, 2629 HS Delft, the Netherlands

Sander J. Heblij[b], and Dick H. T. Bergmans[c]
Netherlands Aerospace Centre, 1059 CM Amsterdam, the Netherlands

Mirjam Snellen[d] and Dick G. Simons[e]
Delft University of Technology, 2629 HS Delft, the Netherlands

Accurate predictions of aircraft noise levels are desirable to enforce noise control regulations around airports and to evaluate noise abatement procedures. The current best practice noise contour prediction models assume certain default net thrust values depending on the engine type and aircraft altitude. This paper proposes a method for calculating the engine fan settings, $N1\%$, (and hence, the net thrust) directly from audio recordings. This method was tested with a large number of Airbus A330–300 and Boeing 777–200 flyover audio recordings. A significant correlation was found between the recorded noise levels and $N1\%$, explaining up to 45% of the variability in the noise levels. Using the calculated $N1\%$ values in the noise prediction models, instead of the default values, increases the agreement with the actual recorded noise levels and explains parts of the variability. The inclusion of accurate values of $N1\%$ and the update of the aircraft noise prediction calculations is, therefore, highly encouraged, for example by increasing the dependency on $N1\%$ of the noise levels.

[a] PhD candidate, Aircraft Noise & Climate Effects section, Faculty of Aerospace Engineering, Kluyverweg 1. AIAA Student Member. E-mail: r.merinomartinez@tudelft.nl

[b] R&D engineer, Environment & Policy support, Anthony Fokkerweg 2. E-mail: sander.heblij@nlr.nl

[c] R&D engineer, Environment & Policy support, Anthony Fokkerweg 2.

[d] Associate professor, Aircraft Noise & Climate Effects section, Faculty of Aerospace Engineering, Kluyverweg 1. E-mail: m.snellen@tudelft.nl

[e] Full professor, Aircraft Noise & Climate Effects section, Faculty of Aerospace Engineering, Kluyverweg 1. E-mail: d.g.simons@tudelft.nl

I. Introduction

As aircraft noise becomes an increasingly important issue due to the continuous growth in air traffic [1], obtaining accurate knowledge of aircraft noise levels is desired for reliably enforcing environmental laws in the vicinity of airports. These calculations are employed for land–use planning and management worldwide.

The current practice to estimate aircraft noise levels is typically based on legal compliance methods such as those described in Document 29 of the ECAC (European Civil Aviation Conference) [2]. Using such methods, noise contours around airports can be calculated to represent the noise impact of aircraft operations over a period of time. Hence, these contours are often employed to set noise limits, estimate future aircraft impact, and for law enforcement purposes. The methodology of ECAC's Doc. 29 can be called best practice: relatively large assumptions are made, either for practical reasons or due to the lack of detailed data. The noise levels are estimated for each operation using look–up tables, such as the noise–power–distance (NPD) tables, whereby the aircraft thrust settings and distance to the observer are key inputs. After determining the noise levels from these tables for a specific observer position, corrections such as lateral attenuation, segment event level corrections, installation effects, and bank angle effects may apply. Previous comparisons between aircraft noise prediction models and experimental measurements [3, 4] showed that considerable errors are made by the models due to the large assumptions considered within their calculations. Therefore, experimental validations and potential improvements of these models are highly recommended.

Other more sophisticated, semi–empirical prediction models, such as ANOPP [5], PANAM [6] or SIMUL [7] describe the sound emission and propagation separately and offer more detailed predictions but they require very detailed input data, which are not typically publicly available and their database is limited to a small number of aircraft [4]. In addition, these programs are not accessible to other users. Therefore, this paper focuses on the best practice method of Doc. 29.

These simpler best practice prediction tools, such as the NPD tables, provide a single noise level for a certain aircraft type, in a certain flight phase and at a specific distance from the observer [2, 8–11]. Previous research [12–16] showed that changes in certain aircraft settings (especially

the fan rotational speed) produce variations in the noise levels of several decibels. Zellmann *et al.* [4] showed that the dependency between the noise levels and the fan rotational speed can be modeled using second–order polynomials, depending on the frequency and the emission direction. Not accounting for this fact can considerably hamper an accurate calculation of noise contours. The noise prediction models employ estimations for the net engine thrust, which are normally provided as input by the user via a standard thrust profile (i.e., for different flight phases). As an example, the noise levels predicted for the Boeing 777–200 aircraft type equipped with GE90–76B engines are depicted in Fig. 1a. The curves corresponding to different net engine thrusts are presented, where the noise levels are plotted against the distance. The data from Fig. 1a were obtained from the international Aircraft Noise and Performance (ANP) database [17].

In order to assess the current assumptions regarding net thrust of the noise contour models, the actual engine settings (i.e., the relative fan rotational speed) and the distance between the aircraft and the observer need to be determined. Whereas the actual aircraft settings are recorded by airlines using the aircraft flight movement system, these data are not publicly available for reasons such as pilot privacy and to ensure the operation business strategies of the airlines. To counteract this lack of information, a methodology to determine the engine fan settings based solely on audio files is proposed and described in this paper. Whereas some of the aforementioned studies [3, 13–16, 18–20] made use of phased microphone arrays to separate and analyze the noise contributions of different aircraft components, the present research only considers the total aircraft noise levels recorded by individual microphones from the Noise Monitoring Terminals (NMT) of the Noise Monitoring System (NOMOS) around Amsterdam Airport Schiphol in the Netherlands.

The focus of this paper is, therefore, on investigating the flight–phase–dependent engine settings and their effect on the predicted noise levels. For that purpose, a large set of experimental data, containing more than one thousand flyovers of Airbus A330–300 (henceforth Airbus 333) and Boeing 777–200 (henceforth Boeing 772) aircraft under different operational modes (arrivals and departures), was analyzed to compare the engine fan settings considered by the models with those found experimentally. A correlation analysis was performed between the recorded noise levels, the measured engine fan settings and the aircraft velocity to assess the importance of those two param-

eters on the aircraft noise levels. Finally, a comparison between the noise levels predicted based on the NPD tables and those recorded experimentally is also presented.

This paper is structured as follows: Section II briefly explains the noise prediction model considered. Section III contains the details of the experimental setup and the dataset employed in this research. Section IV explains the empirical method used to estimate the aircraft engine fan settings. Finally, section V presents the obtained results and section VI gathers the main conclusions drawn.

II. Noise prediction model

The aim of this research is to investigate the effects of considering the instantaneous thrust setting on the noise level predictions by the noise contour models, rather than employing tabulated values as in practice. The models predict the noise levels perceived at a certain distance from the aircraft, depending on the thrust setting employed. In particular, NPD tables usually require the corrected net thrust per engine $\frac{F_n}{\delta}$ as an input, which can be calculated using the following equation

$$\frac{F_n}{\delta} = E_0 + F_0 V_C + G_A h + G_B h^2 + HT + K_3 \left(\frac{N1\%}{\sqrt{\theta_T}}\right) + K_4 \left(\frac{N1\%}{\sqrt{\theta_T}}\right)^2, \tag{1}$$

where F_n is the net thrust per engine in lbf, δ is the ratio between the ambient air pressure at the aircraft to the standard air pressure at mean sea level (101,325 Pa), V_C is the calibrated airspeed in kts, h is the aircraft altitude in ft and T is the ambient air temperature in which the aircraft is operating in °C. The parameter $N1\%$ refers to the engine fan rotational speed (explained later in detail in section IV B) and θ_T is the ratio between the absolute total temperature at the engine inlet to the standard air temperature at mean sea level (288.15 K). The constants K_3 and K_4 are derived from the installed engine data encompassing the $N1\%$ values of interest. The variables E_0, F_0, G_A, G_B and H are engine constants for temperatures below the engine flat rating temperature at the thrust rating in use, obtainable from the ANP database [17] for most aircraft types (except turbojet aircraft). The unit of the corrected net thrust obtained with Eq. (1) is lbf.

Once the corrected net thrust per engine $\frac{F_n}{\delta}$ is known, it is introduced in the NPD tables, where it is interpolated (or extrapolated) linearly within the available data (cells in the table). Afterwards, the selected distance is introduced in the table and interpolated (or extrapolated) logarithmically

to obtain the estimated noise level at that distance from the aircraft. An example of an NPD table is depicted in Table 1, which contains the available data used in this research for the Airbus 333 (equipped with CF6–80E1A engines) and Boeing 772 (equipped with GE90–76B engines) aircraft types. The first column denotes the aircraft type and operation mode (approach (Ap) or departure (Dep)), the second column contains the corrected net thrust per engine $\frac{F_n}{\delta}$ and the last block of columns represents the $L_{\mathrm{p,A,max}}$ values in dBA for each distance r in ft, as specified in the first row. The graphical representation of these values for departures of the Boeing 772 type equipped with GE90 engines (last 6 rows in Table 1) are presented in Fig. 1a. In Fig. 1 one klbf is equivalent to 4.448 kN.

As aforementioned, one of the main issues of the noise prediction models is that the actual value of $N1\%$ (and hence of the net thrust) is not disclosed in practice and estimations need to be made. Figure 1b depicts typical corrected net thrust profiles (per engine) for both aircraft types during departure and arrival, depending on the altitude [17]. The respective engine fan rotational speed values can be calculated solving Eq. (1) for $N1\%$. It should be noted that several thrust profiles are used for departures in practice, depending on the assumed takeoff weight of the flight, typically categorized in so–called stage lengths, but for the altitudes considered in this research, the differences between thrust profiles were negligible for all stage lengths considered (third to eighth). On the other hand, a single approach thrust profile per aircraft type is normally employed. The altitudes of the flyovers considered in this study are located in the *plateaus* in Fig. 1b before (on the left of) the cutback points, which correspond to altitudes of 1500 ft for departures and of 1000 ft for arrivals. Therefore, the estimated thrust values are practically constant for the whole altitude range, within each aircraft type and operation mode. However, previous studies [12–16] confirmed that, in practice, large variations in $N1\%$ occur at the same distance to the observer. The operational reasons why $N1\%$ vary are because pilots and airlines make use of reduced thrust to extend maintenance intervals and that automatic thrust settings control the aircraft to follow the glide path under the influence of wind gust and to maintain constant landing velocity. Hence, there is a clear interest in obtaining the actual $N1\%$ values of the aircraft.

An additional consideration and premise about this prediction model that should be noted is

Table 1: NPD table for the A333 and B772 aircraft types. "Ap" denotes approach and "Dep" denotes departure. The third block of columns represent the $L_{\mathrm{p,A,max}}$ values in dBA for each distance r in ft. Adapted from [17].

		r, [ft]									
Type	$\frac{F_n}{\delta}$, [lbf]	200	400	630	1000	2000	4000	6300	10000	16000	25000
A333 Ap	6000	93.8	86.6	82	77.2	69.6	61.4	55.4	48.7	41.1	33
A333 Ap	12000	96.7	89.2	84.3	79.1	71	62.4	56.2	49.2	41.6	33.5
A333 Dep	34000	105.5	97.4	92	86.3	77.7	68.4	61.8	54.3	46.2	37.4
A333 Dep	42000	106	98.2	93.2	88	79.8	70.7	64.2	56.9	48.8	40.1
A333 Dep	52000	107.5	100.1	95.2	90.2	82.3	73.8	67.6	60.6	52.7	44
A333 Dep	62000	111.7	104.4	99.6	94.5	86.6	78.4	72.4	65.6	57.6	48.8
B772 Ap	12000	94.2	86.8	81.8	76.8	68.9	60.3	54.1	47.5	40.8	34.5
B772 Ap	17000	95.3	87.9	82.9	77.9	69.9	61.2	55	48.3	41.5	35.1
B772 Ap	22000	96.6	89	84	78.9	70.7	62	55.6	48.9	42	35.6
B772 Ap	27000	97.9	90	84.9	79.7	71.4	62.5	56.2	49.4	42.5	36
B772 Dep	31000	97.5	90.7	86	80.8	72.8	63.8	57.5	50.4	43.3	36.4
B772 Dep	41000	98.8	92	87.3	82.2	74.2	65.3	59	52.1	45.1	38.4
B772 Dep	51000	100.6	93.8	89.2	84.1	76.2	67.3	61.1	54.3	47.5	40.9
B772 Dep	61000	102.8	96	91.4	86.4	78.5	69.7	63.6	56.9	50.1	43.5
B772 Dep	71000	105	98.3	93.7	88.7	80.8	72.1	66.1	59.4	52.7	46.3
B772 Dep	81000	109	102.4	97.8	92.9	85.2	76.7	70.8	64.4	58	52

that, according to the Document 29 of the ECAC [2], "*this methodology applies only to long–term average noise exposure; it cannot be relied upon to predict with any accuracy the absolute level of noise from a single aircraft movement and should not be used for that purpose*". Thus, the aim of this research is to extend the model capabilities for predicting the noise levels of single events and to account for the inherent variability in the noise levels observed, which can lead to important errors when assessing the annoyance experience by the population living around airports.

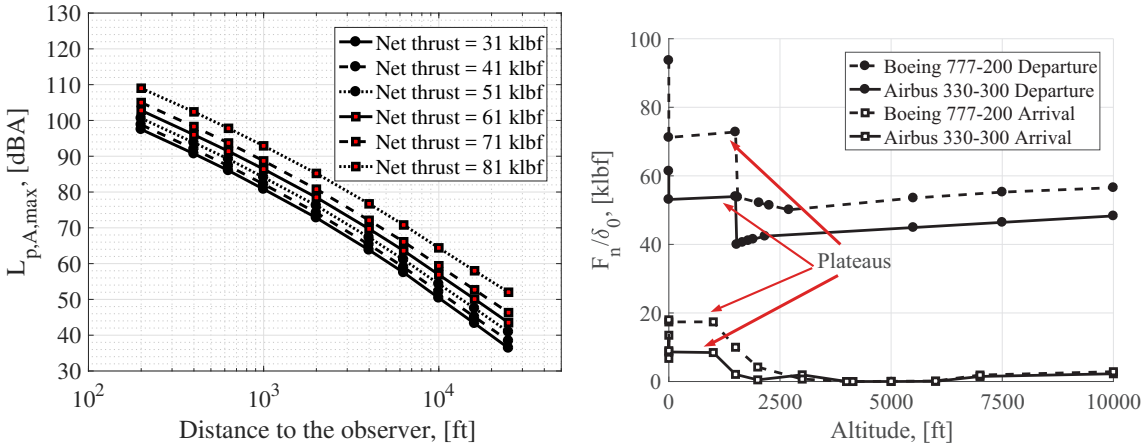

(a) (b)

Fig. 1: (a) NPD noise level estimations for B772 departures. (b) $\frac{F_n}{\delta}$ estimations for example flight profiles [17].

Table 2: NMT locations.

NMT number	Address	Latitude, [deg]	Longitude, [deg]	Altitude, [m]
01	Kluyperlaan 30, Zwanenburg	52.3784122	4.7400112	-2
10	Clusiusstraat 23, Aalsmeer	52.2631668	4.7732408	-3
14	Hoofdweg 1730, Abbenes	52.2353764	4.5937646	-3

III. Experimental setup

To get a statistically significant analysis, a dataset containing many aircraft flights is considered. The study is based on 1121 audio files recorded by three different NMTs in the vicinity of Amsterdam Airport Schiphol in 2016. These flyovers correspond to arrivals and departures of two aircraft types: Airbus 333 and Boeing 772. Both aircraft are wide–body twin–engine jet airliners of comparable size (see Fig. 2), but the Airbus 333 is designed for medium– to long–range operations, whereas the Boeing 772, with higher weight and thrust, is intended for long–range purposes. It can be observed in Fig. 1b that the Boeing 772 normally has higher corrected net thrust values than the Airbus 333.

The locations of the selected three NMTs (out of the 31 NMTs available) used for this research (01, 10 and 14) are highlighted in red in Fig. 3, whereas their coordinates are presented in Table 2.

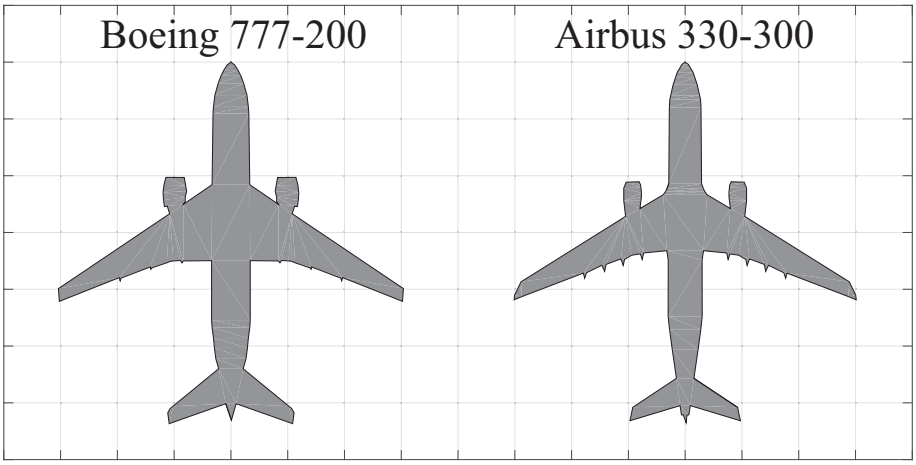

Fig. 2: Aircraft contours of the B772 (left) and A333 (right). The grid step is 10 m.

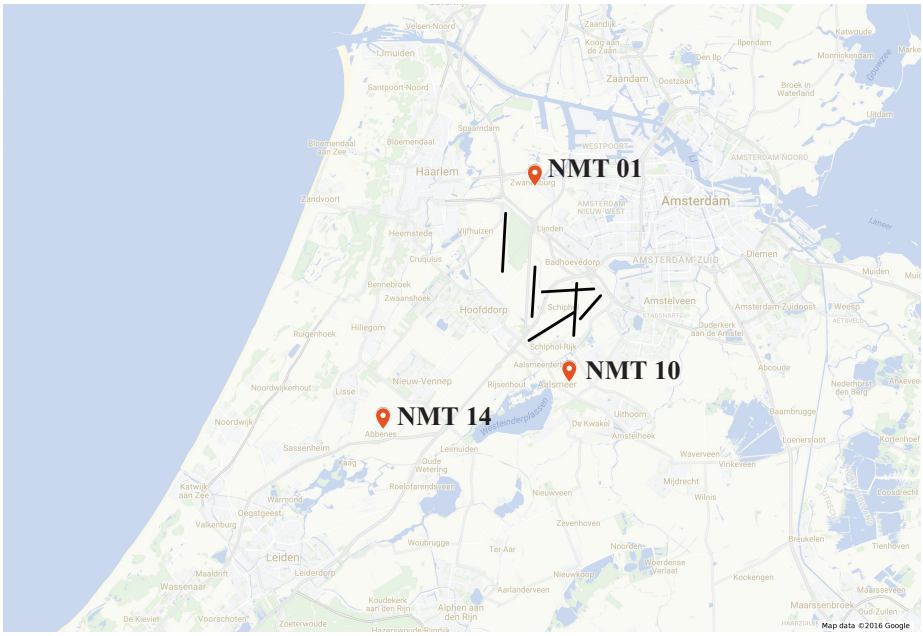

Fig. 3: NMTs 01, 10 and 14 and airport runways (black lines). Map obtained using Google Maps.

The airport runways are denoted as black lines. The positions of the NMTs have been selected in order to include a representative number of both arrivals and departures.

The NOMOS system has been active since 1993 in residential areas around this airport. Each of the NMT has a calibrated microphone which continuously measures the noise in the area. The microphones employed are part of the Brüel & Kjær airport noise monitoring and management system [21]. The microphones start recording whenever a certain threshold sound pressure level (L_{p}) is exceeded and measured. Normally, the trigger cause corresponds to an aircraft flyover, but

Table 3: Number of flyovers selected for each NMT and each aircraft type.

NMT number	Airbus 333 flyovers	Boeing 772 flyovers	Subtotal per NMT
01 (Approach)	96	63	159
10 (Departure)	94	133	227
14 (Approach)	221	185	406
14 (Departure)	212	117	329
TOTAL	**623**	**498**	**1121**

sometimes other sound sources, such as birds tweeting nearby or a church bell ringing, also trigger the recording, and need to be rejected. This system provides the recorded noise levels on–line to the public [22] and the raw data upon request. The recorded noise metrics, e.g. the maximum Overall A–weighted Sound Pressure Level ($L_{\mathrm{p,A,max}}$ or $\mathrm{OASPL_{max}}$) or the Sound Exposure Level ($L_{\mathrm{p,A,e}}$ or SEL) of a specific event can also be traced back to the recorded audio files.

Unfortunately, to reduce data storage, the NOMOS audio files are filtered and resampled with a sampling frequency of 8 kHz when stored. This causes a loss of information [23] and errors when calculating the noise metrics with the audio files available, since all the spectral information is lost for frequencies higher than 3500 Hz. Therefore, it was decided to only consider the recorded noise metrics by NOMOS (before the data compression) as a reference. Therefore, it was decided to only consider the recorded noise metrics by NOMOS (before the data compression) as a reference. Henceforth, the $L_{\mathrm{p,A,max}}$ metric is considered in this study. Additional metrics recorded by NOMOS, such as the $L_{\mathrm{p,A,e}}$ and the Effective Perceived Noise Level (EPNL), showed a very strong and significant correlation (with correlation coefficients $\rho > 0.9$) with the $L_{\mathrm{p,A,max}}$. Therefore, the conclusions presented afterwards in the correlation analysis with $L_{\mathrm{p,A,max}}$ (Sec.V B) can be extended to these other metrics.

Table 3 divides the total number of flyovers depending on the aircraft type, the NMT that recorded the measurement and whether the operation mode was an approach or a departure. A total of 623 Airbus 333 and 498 Boeing 772 flyovers were recorded. The number of approaches (565) was similar to the number of departures (556).

Since not all the aircraft recorded had the same engine type, Table 4 contains an overview of the number of aircraft equipped with each engine type, as well as the number of fan blades, B, and the maximum fan rotational speed at 100% engine fan setting, $n_{\max}$. The minimum and maximum EPNL certification values for approach for each engine type (obtained from [24]) are also indicated in the last column for illustration purposes. Variation ranges in EPNL between 0.2 and 1.2 EPNdB are observed within the same engine type, due to small modifications by the manufacturers [24]. These differences are deemed to be negligible compared to the variability ranges found in practice [13, 15]. Different engine types from the same family can be grouped in a same category, provided that they have the same values for B and $n_{\max}$ (see Table 4). The EPNL certification values for each category are practically identical. Thus, the Airbus 333 flyovers are divided into four categories: CF6–80E1A (387 cases), PW4168A (179 cases), PW4170 (17 cases) and TRENT 772 (40 cases); whereas the Boeing 772 flyovers are divided into two categories: GE90 (496 cases) and TRENT 892 (2 cases).

The trajectories of the aircraft flyovers were determined using radar data from air traffic control and referenced to the coordinates of the respective NMT. The position data are recorded every 4 seconds and interpolated linearly in between. Hence, the aircraft velocities and the distances to the observer over time are approximately known. The x, y and z coordinates considered in this paper are relative to the respective NMT coordinates. Figure 4a shows an example of the aircraft flyover trajectories for the approaches recorded by the NMT 01 (denoted by a red dot), confirming that the flight paths during approach are relatively uniform, since all aircraft follow the instrument landing system approach. Figure 4b contains a box plot of the minimum distances of each flyover to each of the four NMT cases, where a distinction is made between approaches (Ap) and departures (Dep). On each box, the central mark is the median, the edges of the box are the 25^{th} and the 75^{th} percentiles and the whiskers extend to the most extreme data points. It can be observed that the minimum distances for departure maneuvers are indeed more variable than landings. The average minimum distance to the observer (NMT station) for all measurements was 790 m.

Since, as shown in Fig. 4b, the (minimum) distances from each aircraft to the respective NMT show differences, a correction in the measured noise levels was performed to correct for the varying

Table 4: Aircraft types with their corresponding engine and number of recorded measurements for each type. The minimum and maximum EPNL certification values for approach for each engine type are also indicated.

Aircraft type	Engine type	Number	Fan blades, B	$n_{\max}$, [rpm]	$\Delta\text{EPNL}_{\text{Ap}}$, [EPNdB]
Airbus 333	CF6–80E1A3	169	38	3320	[99.1 - 99.6]
	CF6–80E1A4	79	38	3320	[99.1 - 99.6]
	CF6–80E1A4B	139	38	3320	[99.1 - 99.6]
	PW4168A	179	34	3600	[97.9 - 98.7]
	PW4170	17	34	3680	[98.1 - 98.7]
	TRENT 772	21	26	3900	[96.7 - 97]
	TRENT 772B–60	19	26	3900	[96.7 - 97]
Boeing 772	GE90–90B DAC I	23	22	2262	[97.6 - 98.8]
	GE90–92B	2	22	2262	Not found
	GE90–92B DAC I	3	22	2262	Not found
	GE90–94B	468	22	2262	[98.4 - 98.8]
	RB211 TRENT 892	2	24	3300	[99.9 - 100.1]

effect of sound spreadings, in order to study all aircraft in similar conditions. For each of the four NMT cases the mean minimum distance ($\bar{r}_{\min}$) to each NMT for all the recorded flyovers was calculated. A correction value ΔL_{p} was added to the noise metrics from the measurements of all flyovers depending on their respective minimum distance to the NMT ($r_{\min}$), given by the following formula

$$\Delta L_{\text{p}} = 20 \log \left(\frac{r_{\min}}{\bar{r}_{\min}} \right). \tag{2}$$

Note that ΔL_{p} is negative for $r_{\min} < \bar{r}_{\min}$ and positive for $r_{\min} > \bar{r}_{\min}$. This means that for aircraft flying further away than the $\bar{r}_{\min}$ the values of their noise levels will increase and vice versa. Hence, the effect of having different measuring distances is at least partially accounted for.

Due to the limited frequency range available in the audio recordings (only up to 3500 Hz),

the effect of the atmospheric absorption on sound was not accounted for, since the effect of the atmospheric absorption is specially notable for high frequencies. Hence, the relative effect of the atmospheric absorption on each flyover with respect to the effect at the mean distance $\bar{r}_{\min}$ is expected to be small for the frequency range available. However, the full frequency range was used when calculating the $L_{\mathrm{p,A,max}}$ values by NOMOS. The NPD tables account for an average effect of the atmospheric absorption, depending on the distance to the observer.

The experimental data was continuously recorded during a two–month period, with relatively similar weather conditions. The weather data was recorded hourly by the Royal Netherlands Meteorological Institute (KNMI) [25]. The local temperatures were used for estimating the sound speed and for the required parameters in Eq. (1). The recorded wind speeds were taken into account to use the true airspeeds of the aircraft, which are employed henceforth in this paper.

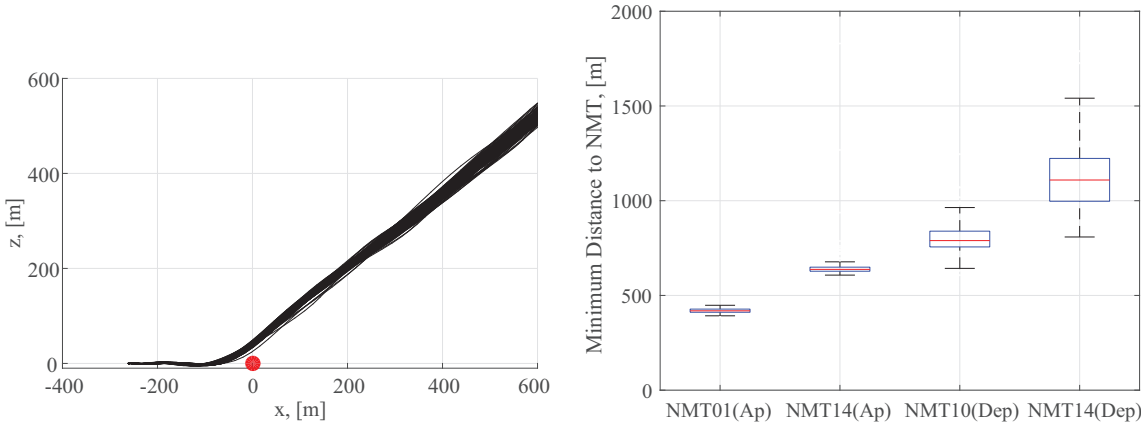

(a) (b)

Fig. 4: (a) Recorded approaches trajectories at NMT 01. (b) Box plot of the minimum distances to each NMT.

IV. Estimation of the aircraft engine settings

A. Physical considerations about the acoustic data

The Doppler effect due to the relative motion of the aircraft with respect to the observer needs to be considered for the fan rotational speed estimation. The expression for the Doppler–shifted frequency, f', is

$$f' = \frac{f}{1 - \|\boldsymbol{M}\| \cos(\theta)}\,, \tag{3}$$

where $\|\cdot\|$ is the Euclidean norm of the vector, f' is the observed frequency, f is the emitted frequency, $\boldsymbol{M}$ is the Mach number vector, $\boldsymbol{M} = \boldsymbol{V}/c$, $\boldsymbol{V}$ is the source velocity vector, c is the speed of sound and θ is the angle between the relative position vector of the source with respect to the observer, $\boldsymbol{r}$, and the source velocity vector, $\boldsymbol{V}$, see Fig. 5. The Doppler effect can be observed in the varying frequency of the engine fan tones in the spectrograms shown in Fig. 8.

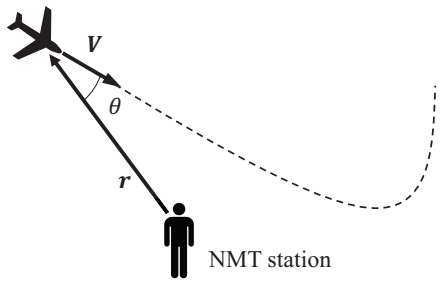

Fig. 5: Diagram explaining the relative movement of the aircraft with respect to the observer.

B. Fan noise analysis

The rotation of the turbofan generates tonal sound due to the interaction between the fan blades and the stator vanes, which is specially noticeable in the forward direction [15, 23] (i.e., for $\theta < 90°$ in Fig. 5). The fundamental frequency of this sound, f_1, is called blade passing frequency (BPF) and is calculated as:

$$\text{BPF} = f_1 = \frac{B\,n}{60}\,, \tag{4}$$

where B is the number of fan blades (as introduced in Table 4) and n is the fan rotational speed in revolutions per minute. Thus, the fan rotational speed can be determined from the audio files.

Higher harmonics of the BPF are usually found as well in the sound of aircraft flyovers. The frequencies of these harmonics, f_k, are multiples of the BPF (f_1):

$$f_k = k\,f_1, \;\; k = 1,\, 2,\, 3\ldots\,. \tag{5}$$

Unfortunately, due to the resampling of the available audio data and the consequent low maximum frequency (3500 Hz), few higher harmonics were found in the spectrograms in practice.

The term *engine fan setting* [3, 14–16] typically refers to the ratio between the fan rotational speed, n, and the maximum fan rotational speed, $n_{\max}$ (see Table 4). This relative fan percentage speed is normally denoted as $N1\% = 100\, n/n_{\max}$ because it refers to the low–pressure shaft of the engine, on which the fan is mounted. In contrast to the thrust or the jet velocity of the engine, it can be directly measured [4]. The expected value of $N1\%$ during approach is considerably lower than during departure because of the descent. In addition, turbofan aircraft during departure can present the so–called *buzz–saw* noise produced at the tip of the fan blades when they reach supersonic speeds, thus, producing shock waves [23]. These tones are harmonics of the engine shaft rotation frequency, which is typically considerably lower than the BPF. Therefore, additional care needs to be taken when analyzing aircraft tonal noise during departure to only consider fan tones and not *buzz–saw* tones.

The first step in this analysis is, thus, to determine the BPF value for each flyover audio recording and then calculate the fan rotational speed n using Eq. (4). The flowchart presented in Fig. 6 shows the inputs necessary for this method: the trajectory and engine characteristics of the aircraft (Table 4) and the audio recording of the flyover. The expected Doppler shift can be estimated using the aircraft trajectory and Eq. (3). Afterwards, a least–squares curve–fitting process [26] is performed in order to find narrow–band engine fan tones in the signal spectrogram that agree with the calculated Doppler shift. The spectrograms are calculated by using 2048 samples per time block with Hanning windowing and a 50% data overlap. For each time step, peaks over a certain threshold are considered. Afterwards, the characteristic Doppler–shifted curves corresponding to the fan tonal noise were searched for using these peaks, considering the expected Doppler shift as calculated from the aircraft trajectory, according to Eq. (3) and shown in Fig. 7c. First, the BPF is searched for in the spectrogram within a predefined search frequency band over time, depending on the operation mode and engine characteristics. A fitting process was performed to match the detected peaks to the expected continuous and monotonically decreasing Doppler–shift curve. Changes in the engine fan settings performed by the pilot during the recording time or turbulence in the atmosphere

can also cause "bumps" in the curves representing the engine fan tones, which are expected to be monotonically decreasing otherwise, see Fig. 8b. These irregularities can be accounted for by allowing a small increase (or decrease) in the Doppler–shifted tone frequency with respect to time. The allowable increase or decrease is defined by the user. The presence of higher harmonics is also evaluated by searching for multiples of the estimated BPF and serves as a further confirmation that the obtained BPF value is correct. This process provides a (Doppler–corrected) BPF value (for the instant when $r = r_{\min}$) and, therefore, an $N1\%$ value. The obtained $N1\%$ needs to be checked to confirm that it falls within the typical range depending on the aircraft operation (approach or departure). In case the provided $N1\%$ value is not realistic, the whole process is repeated using a different search frequency band for the BPF. Henceforth, for consistency, the selected instant for studying the value of $N1\%$ was chosen to be when the aircraft is located at the minimum distance $r_{\min}$ to the NMT.

Similar methods can be found in literature [14–16], in which frequency filtering can also be applied as preprocessing to improve the search process [27].

The results for an example Airbus 333 approach flyover recorded by NMT 01 are presented in Fig. 7. Figure 7a illustrates the flight path with respect to the NMT (situated at the origin and represented by a red dot). The thick black line corresponds to the period where the audio recording is available. The calculated angle θ between the relative aircraft position vector, $\boldsymbol{r}$, and the source velocity vector, $\boldsymbol{V}$, over that period is presented in Fig. 7b. The 90° angle is shown as a dashed line for reference. Figure 7c contains the calculated Doppler shift during the same period. The spectrogram of the audio signal is shown in Fig. 8. The vertical solid black line represents the time with $r = r_{\min}$. Figure 8a presents with a thick black line the curve fitted to the calculated Doppler shift (from Fig. 7c). Figure 8b depicts the obtained estimates for the locations of the detected Doppler–shifted engine fan tones. For clarity reasons, double dashed lines around the real solution are plotted to show the curves in the spectrogram. This case is especially illustrative, since not only the BPF but the next four harmonics are also clearly detected and marked with dashed lines in Fig. 8b. The time when $r = r_{\min}$ is marked with a solid black vertical line. Unfortunately, due to the limited maximum frequency and the higher atmospheric absorption at higher sound frequencies,

harmonics higher than the fifth are rarely found in the measurements. The presence of "bumps" in the tones can also be observed in Fig. 8, as explained before, most probably due to changes in the engine fan settings by the pilot or to atmospheric turbulence, which are successfully detected by the search method.

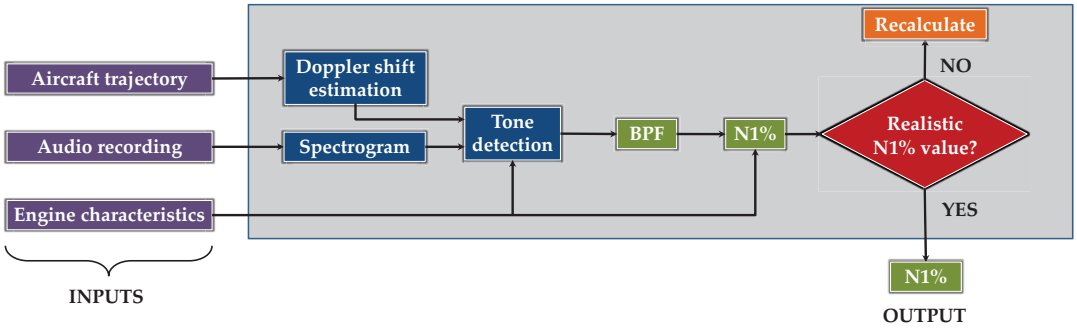

Fig. 6: Flowchart showing the process for estimating the engine fan settings (N1%).

V. Results

For brevity reasons, in the following subsections only results of the data recorded by NMT 14 are presented, since that NMT recorded the highest number of flyovers (406 approaches and 329 departures). Moreover, only the Airbus 333 equipped with engines from the CF6–80E1A family and the Boeing 772 aircraft equipped with engines from the GE90 family are considered. These engines were considered to be the most illustrative types because they were the most frequently occurring, see Table 4. Data from the other NMTs and engine types showed similar results.

A. Comparison between the measured and modeled engine fan settings

The box plots presented in Fig. 9 represent the variability found in several parameters for flyovers recorded by NMT 14. On each box, the central mark is the median, the edges of the box are the 25^{th} and the 75^{th} percentiles and the whiskers extend to the most extreme data points. The outliers are plotted individually as red crosses (+). The results are separated depending on the aircraft type (Airbus 333 or Boeing 772) and the operation mode (approach (Ap) or departure (Dep)):

Figure 9a shows that both aircraft types present higher $N1\%$ values during departure than

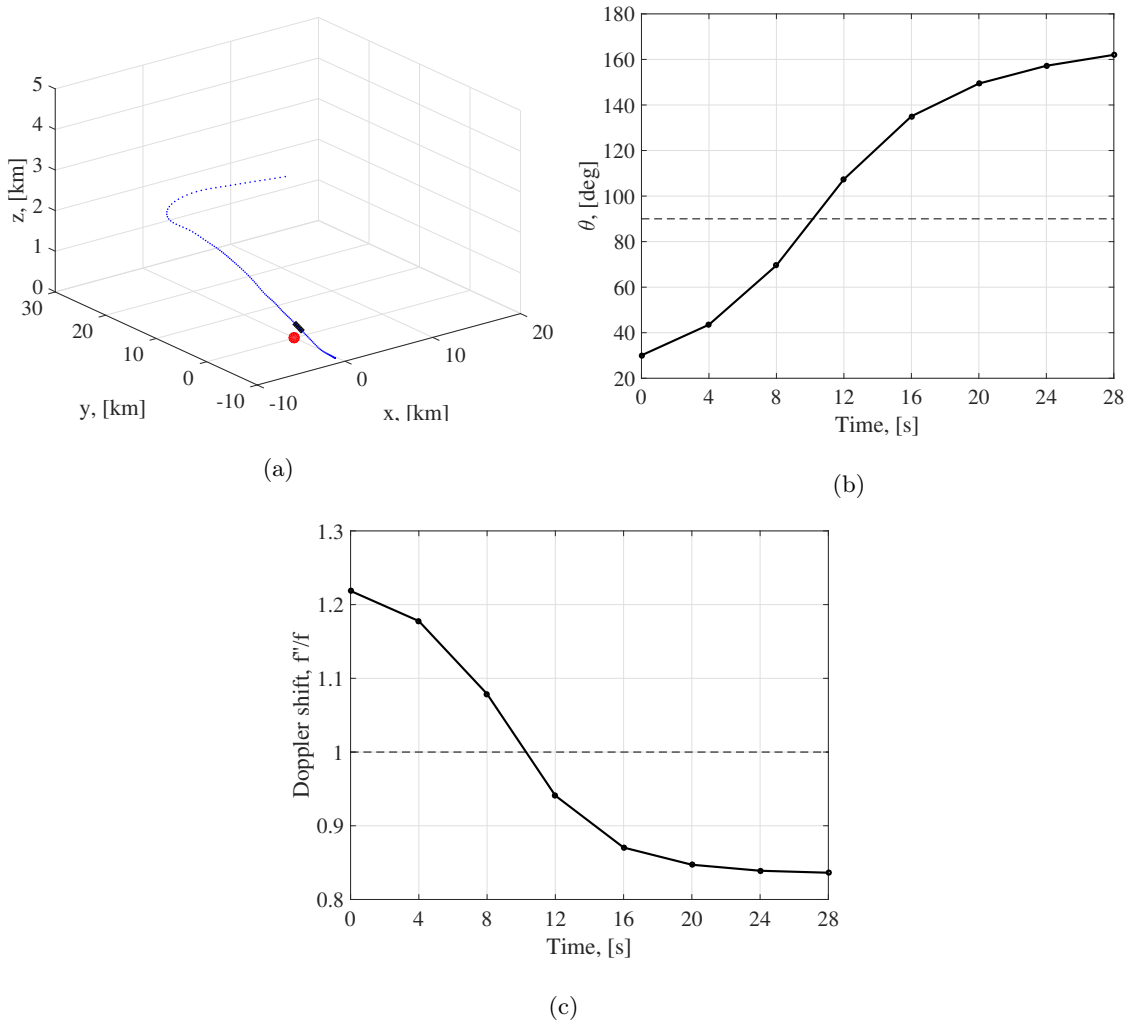

Fig. 7: (a) A333 trajectory. Note the different axes scales. (b) Angle θ and (c) Doppler shift during the recording.

during approach, as expected. However, larger variabilities are found in $N1\%$ during approach, with differences larger than 20%, whereas during departure these differences are roughly 10%. These results indicate that pilots need to adjust the throttle to keep the aircraft on the desired flight path during approach, while for departures the throttle is more fixed. The predicted $N1\%$ values using the data from Fig. 1b and Eq. (1) for these cases are plotted as black dots on the right of each box plot. Since the recorded aircraft correspond to altitudes within the *plateaus* indicated in Fig. 1b, the predicted net thrusts (and hence the $N1\%$) are practically constant per case for the altitude range considered here (see Fig. 1b). The default $N1\%$ values for approach fall inside of the box plots obtained experimentally, although they are comparably lower than the average of these. The

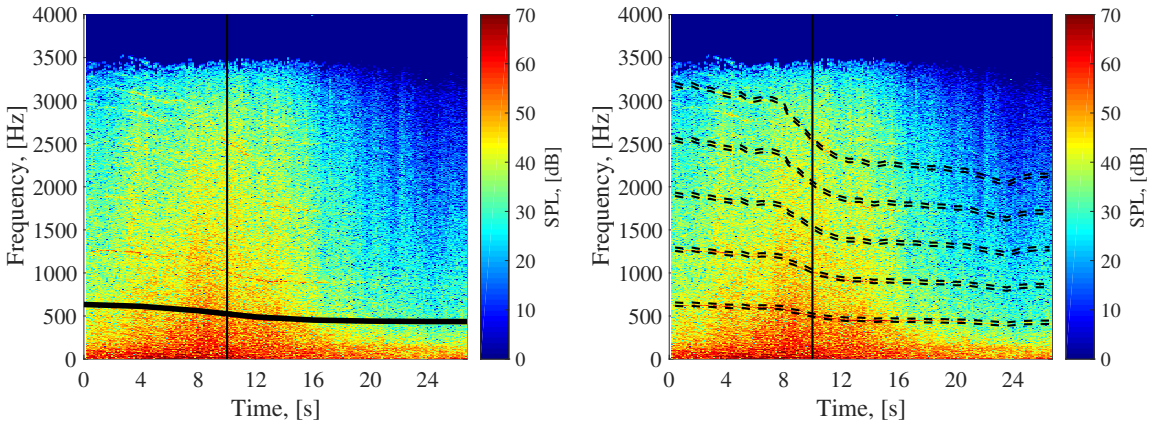

Fig. 8: Spectrograms of the audio signal with: (a) Curve fitted to the Doppler shift. (b) Detected engine tones.

$N1\%$ values for the departures considered by the NPD tables, on the other hand, are slightly higher than the empirical values, i.e., they are slightly overpredicted.

Figure 9b contains the variations in true airspeed for the same cases considered above. The mean aircraft true airspeed is practically constant for the four cases and about 68 m/s. The variabilities of this parameter are also similar for the four cases with variations of about 30 m/s

The box plot in Fig. 9c presents the variations in the $L_{\mathrm{p,A,max}}$ provided by NOMOS (corrected for distance here, as explained in section IV A). The mean values for all four cases are comparable and between 65 and 70 dBA. However, it should be kept in mind that the distance correction explained in section IV A is applied to each operation case individually, considering the corresponding mean minimum distance ($\bar{r}_{\mathrm{min}}$), but the effect of the higher absolute value of $\bar{r}_{\mathrm{min}}$ for departures is not accounted for. Therefore, the reason why departures have comparable $L_{\mathrm{p,A,max}}$ values as approaches is because the $\bar{r}_{\mathrm{min}}$ values for departures is considerably higher (approximately double) than for approaches for NMT 14, see Fig. 4b. In general, variabilities in $L_{\mathrm{p,A,max}}$ of about 20 dBA are observed in the four cases. Thus, it is confirmed that the inherent variabilities in the noise levels for the same aircraft and engine type due to manufacturer modifications, as observed in Table 4, is negligible compared to the variabilities observed in practice.

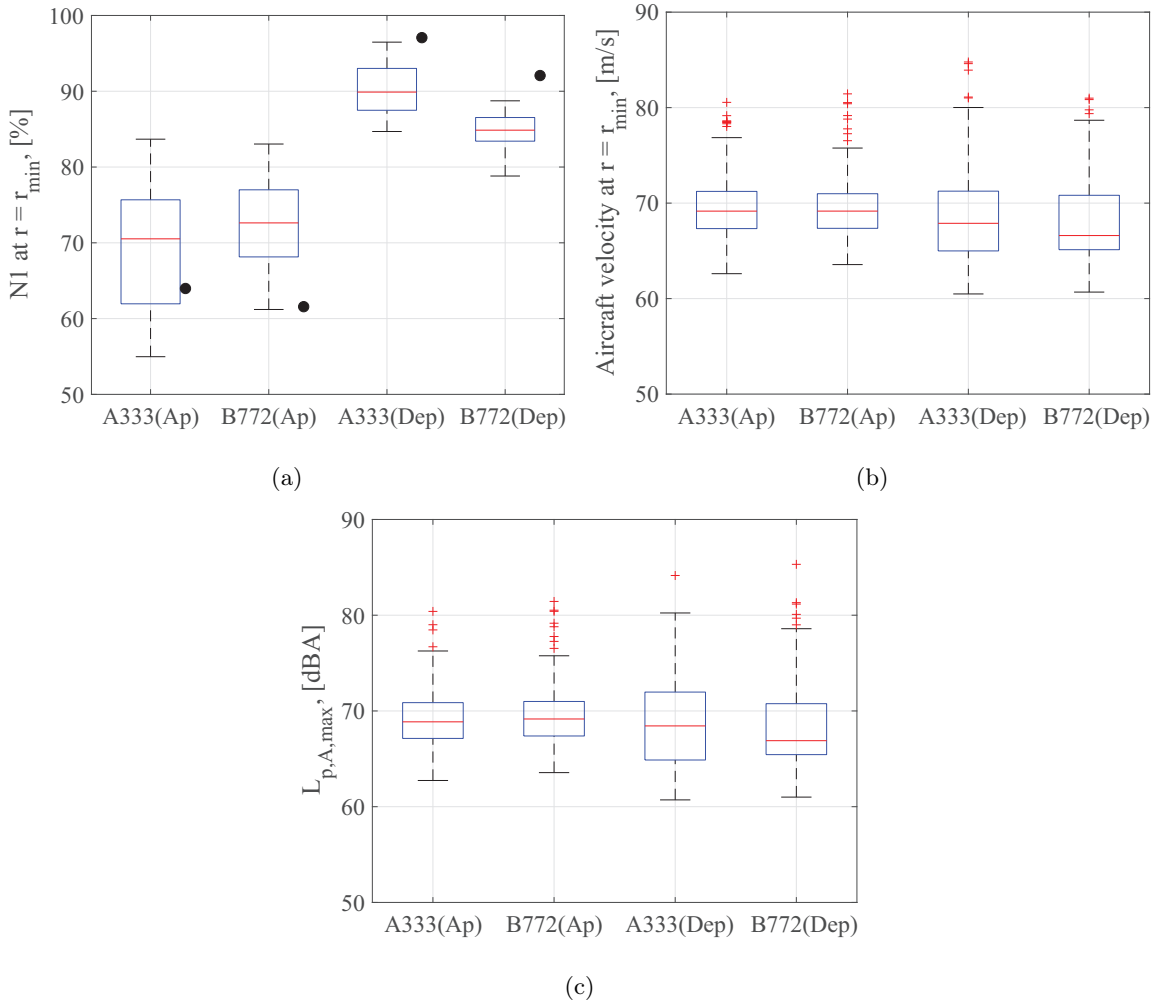

Fig. 9: Box plots for the flyovers recorded by NMT 14 for the: (a) $N1\%$ at $r = r_{\min}$. (b) True airspeeds at $r = r_{\min}$. (c) $L_{\mathrm{p,A,max}}$.

B. Correlation analysis of noise level variations

The results of the correlation analysis between the recorded $L_{\mathrm{p,A,max}}$ by the NMT 14 and the calculated engine fan settings ($N1\%$) at $r = r_{\min}$ for the Airbus 333 and Boeing 772 flyovers in approaches and departures are presented separately in Fig. 10. The correlation coefficient ρ, the coefficient of determination ρ^2 and the p value are included in the legend of each graph. A common criterion to consider a correlation significant is that the p value should be lower than 0.05 [16]. Following this criterion, all the correlations presented in Fig. 10 are deemed as significant. Coefficients of determination between $N1\%$ and $L_{\mathrm{p,A,max}}$ of around 0.3 and 0.4 are found for the approaches of the A333 and B772, respectively. Similar values were obtained by Snellen *et. al.* [15]

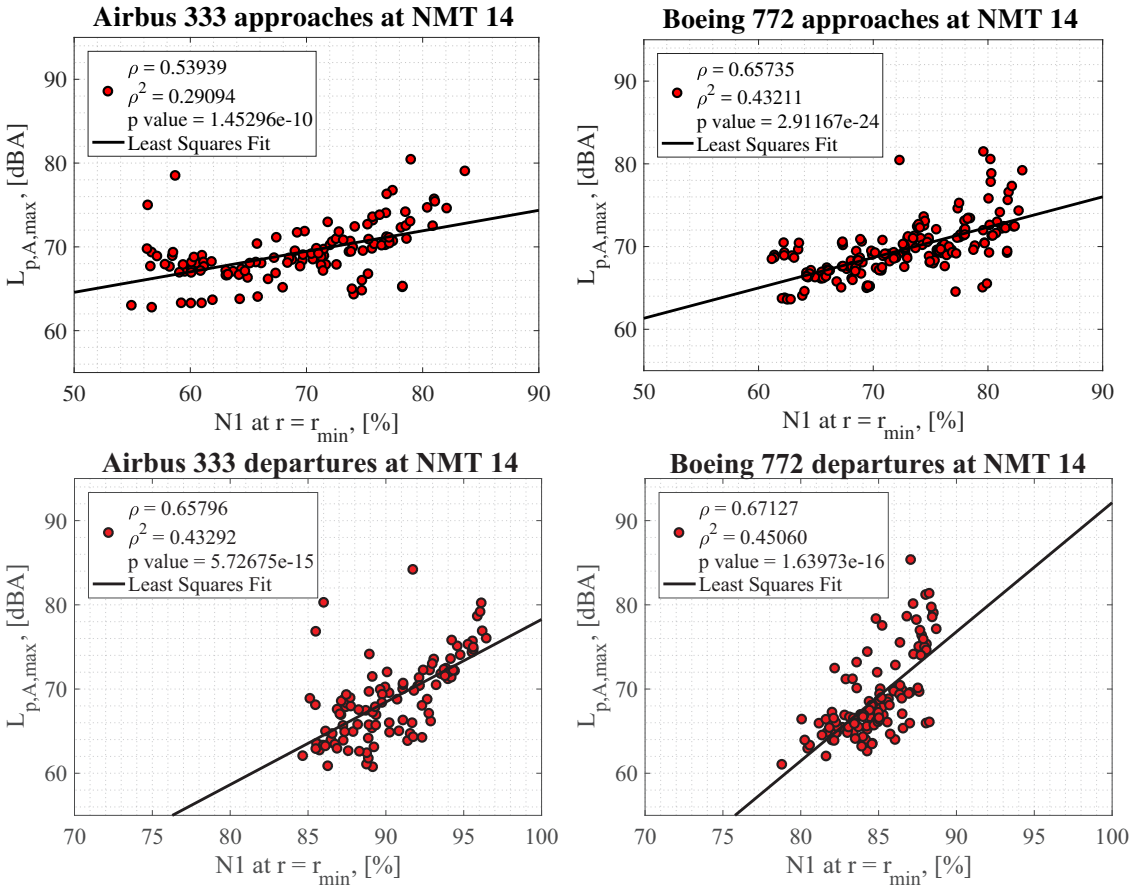

Fig. 10: Correlation analysis between $L_{\mathrm{p,A,max}}$ and $N1\%$ at $r = r_{\mathrm{min}}$ recorded by NMT 14.

for landings of Boeing 737 and Fokker 70 aircraft. Slightly higher values for ρ^2 (around 0.45) are found for the departure operations of both aircraft in the current study. This is expected because engine noise is supposed to be more dominant during departure than during approach [18], so a stronger correlation with the engine fan settings is justified.

The correlation analysis between the recorded $L_{\mathrm{p,A,max}}$ by the NMT 14 and the aircraft true airspeed at $r = r_{\mathrm{min}}$ (not shown in this paper) showed that none of the correlations found between both variables is significant (if the threshold value of 0.05 is again considered for the p value). Thus, it is concluded that, in this research, the aircraft velocity at $r = r_{\mathrm{min}}$ does not seem to influence the $L_{\mathrm{p,A,max}}$ experienced on the ground. The fact that jet noise levels decrease with increasing airspeed [4] could explain the lack of correlation with the airspeed during departure, where jet noise is a dominant noise source. Different results were found by Snellen *et al.* [15], where a significant correlation was found between these two variables for landing aircraft, especially when beamforming

was applied to isolate the noise emissions of certain airframe components, such as the landing gear (reaching ρ values up to 0.8). However in, [15] the minimum distances to the aircraft in that study were considerably smaller (around 70 m) and, thus, the engines are supposed to be operating at lower power settings. Therefore, airframe noise, which has a strong correlation with the flow velocity, becomes more relevant [20]. In addition, the noise levels were considered at the source location, instead of on the ground and more sophisticated sound propagation considerations (such as the atmospheric absorption) were taken into account.

C. Comparison of the recorded noise levels with the modeled ones

In order to assess the importance of including more accurate estimations of the $N1\%$ values obtained with the method explained in section IV compared to the ones used in the NPD tables, a comparison with the recorded NOMOS data was made twice:

1. All the parameters required for Eq. (1) were filled in with the experimentally measured values (V_C, h, T and θ_T), except for $N1\%$ which was determined according to the NPD estimations, using Eq. (1) and Fig. 1b, based on the aircraft altitude.

2. Same conditions as in case 1, but this time the $N1\%$ values used were those found experimentally from the audio recordings as explained in section IV.

It should be noted that the distance correction explained in section IV A was not applied in the $L_{\mathrm{p,A,max}}$ results shown in this subsection, since the NPD tables already account for the effects of the distance to the aircraft (r).

The results of both comparisons with the recorded NOMOS data are gathered in Figs. 11 and 12 for approaches and departures, respectively. In these figures, the graphs on the left correspond to the comparison for the NPD tables predictions using the default $N1\%$ values and the graphs on the right correspond to the comparison for the NPD tables predictions using the $N1\%$ values obtained experimentally. The statistical parameters (correlation coefficient, coefficient of determination and p value) are also shown in each graph. The diagonal line is represented as a black dashed line in Figs. 11 and 12 and represents a perfect agreement between estimated and measured $L_{\mathrm{p,A,max}}$ levels ($\rho = 1$). It can be observed that considering the experimental $N1\%$ values produces a

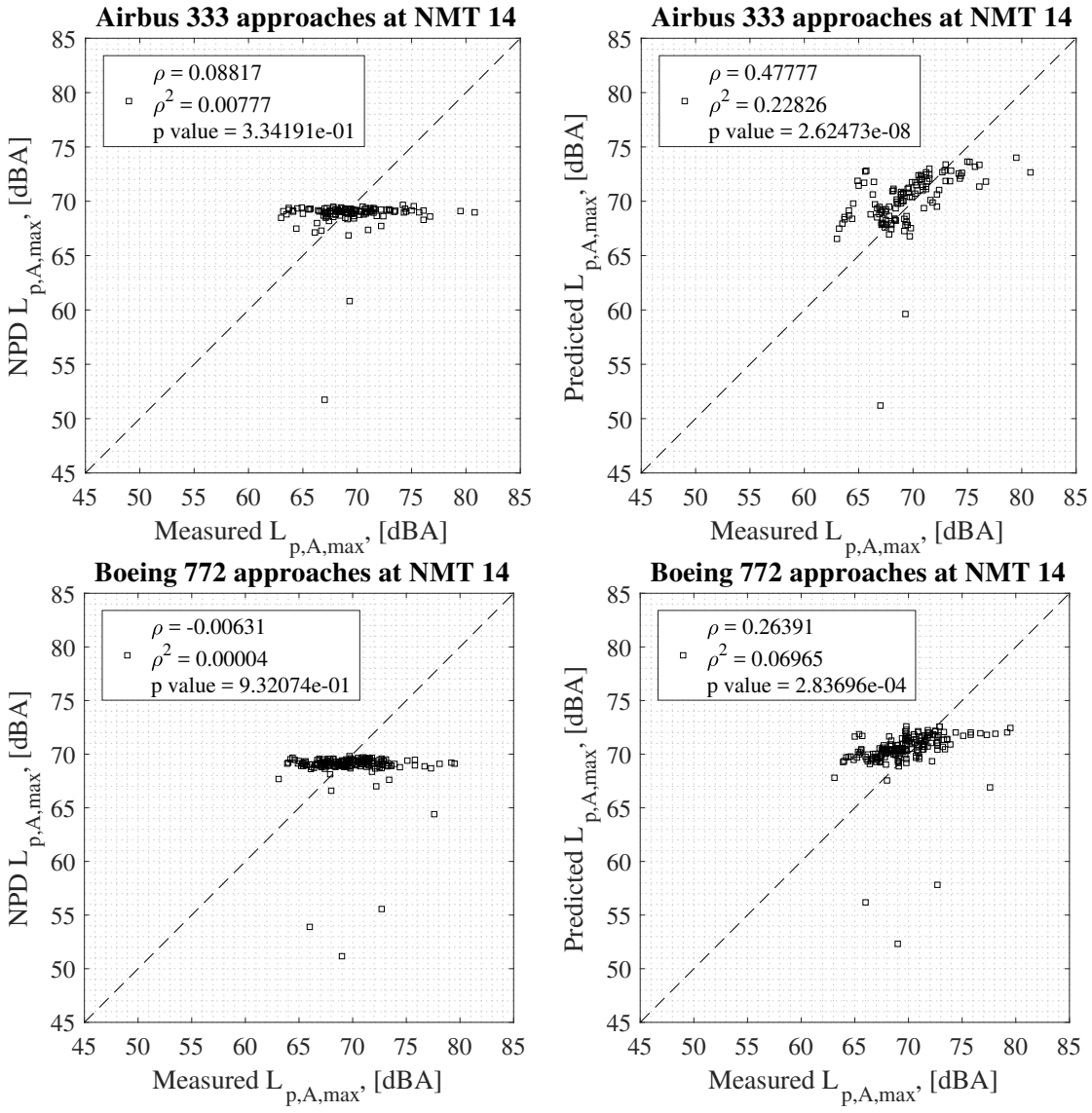

Fig. 11: Recorded $L_{\mathrm{p,A,max}}$ vs. modeled $L_{\mathrm{p,A,max}}$ using default (left) or experimental (right) $N1\%$ values for approaches.

better agreement between the modeled and measured values of $L_{\mathrm{p,A,max}}$. This is confirmed by the considerably higher correlation coefficient values (and hence coefficient of determination values too) presented by the graphs that use the experimental $N1\%$ values. The largest improvement is observed for the case of the Airbus 333 approaches (see, Fig. 11 top graphs) where ρ increases from a value of 0.088 to a value of 0.478.

The average error (ϵ) and the average of the absolute values of the errors (ϵ_{abs}) made by both predictions (using default or calculated $N1\%$ values) for each case are presented in Table 5. The error

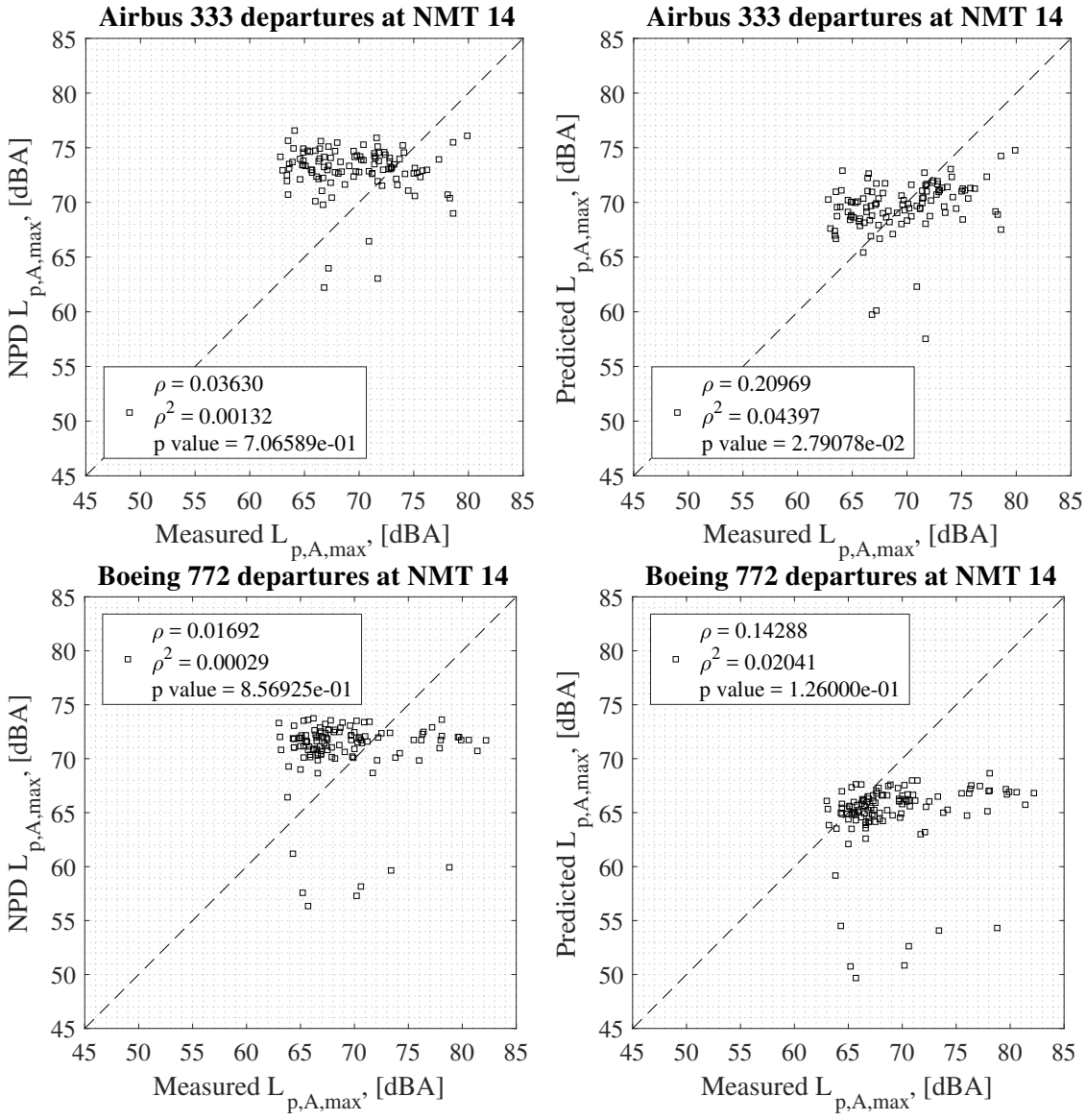

Fig. 12: Recorded $L_{\mathrm{p,A,max}}$ vs. modeled $L_{\mathrm{p,A,max}}$ using default (left) or experimental (right) $N1\%$ values for departures.

is defined as the difference between the measured and the estimated $L_{\mathrm{p,A,max}}$. Hence, $\epsilon > 0$ means that the model underpredicts the actual noise levels and vice versa. The standard deviations of these errors, σ, are gathered in Table 6. On average, including the experimental estimations of $N1\%$ reduces ϵ by 1 dBA and ϵ_{abs} and σ by 0.5 dBA. Despite this improvement, there is still a significant discrepancy between the noise measurements and the noise model predictions. Additionally, it can be observed that in all the graphs there are several outliers that are severely underpredicted by both NPD predictions by up to 15 dBA. These recordings were studied and listened manually and

Table 5: Average error (ϵ) and average of the absolute values of the errors (ϵ_{abs}) for $L_{\text{p,A,max}}$ predictions with the NPD tables' default estimations of $N1\%$ and using the $N1\%$ values obtained experimentally.

Case	ϵ_{NPD}, [dBA]	$\epsilon_{\text{NPD, abs}}$, [dBA]	ϵ_{Exp}, [dBA]	$\epsilon_{\text{Exp, abs}}$, [dBA]
A333 Ap	1.65	2.65	-0.64	2.18
B772 Ap	1.83	2.62	-0.71	2.26
A333 Dep	-2.97	5.38	0.46	3.78
B772 Dep	-1.62	5.00	1.68	3.85

Table 6: Standard deviation (σ) for $L_{\text{p,A,max}}$ predictions with the NPD tables' default estimations of $N1\%$ and using the $N1\%$ values obtained experimentally for each operation case.

Case	σ_{NPD}, [dBA]	σ_{Exp}, [dBA]
A333 Ap	3.58	3.07
B772 Ap	3.57	3.14
A333 Dep	6.05	5.66
B772 Dep	5.62	5.34

it was confirmed that they correspond to aircraft flyovers, but at higher distances to the observer. However, the rest of aircraft parameters, such as velocity or altitude, are normally not determined for the NPD calculations, and default tabulated values are also used. Therefore, the actual NPD estimations for $L_{\text{p,A,max}}$ are most probably less accurate than those presented here. Hence, the error reduction obtained by using accurate $N1\%$ values could be even higher in reality. The approach of including the actual aircraft parameters was taken to isolate the influence of the choice of $N1\%$ for NPD predictions.

Moreover, the variability ranges of the $L_{\text{p,A,max}}$ metric ($\Delta L_{\text{p,A,max}}$, i.e., the maximum $L_{\text{p,A,max}}$ value minus the minimum $L_{\text{p,A,max}}$ value observed) for each dataset (estimations with default or estimated $N1\%$ values or NOMOS recordings) are included in Table 7. For the calculation of this parameter, the aforementioned outliers present in Figs. 11 and 12 were excluded. On average, using

Table 7: $\Delta L_{\mathrm{p,A,max}}$ of (left) the predictions with the NPD tables' estimations of $N1\%$, (center) the predictions using the $N1\%$ values obtained experimentally and (right) NOMOS recordings.

Case	NPD $\Delta L_{\mathrm{p,A,max}}$, [dBA]	Experimental $\Delta L_{\mathrm{p,A,max}}$, [dBA]	NOMOS $\Delta L_{\mathrm{p,A,max}}$, [dBA]
A333 Ap	2.72	7.47	17.80
B772 Ap	3.27	5.69	16.40
A333 Dep	7.87	9.35	17.10
B772 Dep	5.21	6.55	19.20

the experimental estimations of $N1\%$ bring the values of $\Delta L_{\mathrm{p,A,max}}$ 2.5 dBA closer to the NOMOS recordings. Once again, despite this improvement, there is still a remaining 10 dBA variability (on average) that remains unexplained. This additional variability is not accounted for by the prediction model used in this paper, and is subject for future investigation.

VI. Conclusions and outlook

The issue of obtaining accurate predictions of aircraft noise levels was analyzed in this paper. An automatic approach to determine the engine fan settings ($N1\%$) directly from flyover audio recordings was proposed, in order to use more accurate values of this parameter as input for prediction models, rather than tabulated default values. This method was employed on a large data set of more than a thousand aircraft flyovers recorded by the NOMOS system around Amsterdam Airport Schiphol. The aircraft types studied were Airbus A330–300 and Boeing 777–200.

A large spread was found in the values of $N1\%$ obtained experimentally, compared to the default values assumed by the noise models. Significant correlations were found between the calculated $N1\%$ values and the recorded noise levels. On the other hand, no apparent correlation was found between the aircraft true airspeed and the noise levels in this case. Introducing the $N1\%$ values obtained experimentally in the predictions reduced the error made with respect to the NOMOS recordings provided variability values of $\Delta L_{\mathrm{p,A,max}}$ closer to the recorded ones. However, there is still a remaining error and a large variability in the noise levels unexplained by the noise prediction models.

After observing the limitations of the noise prediction model employed in this paper, it is recommended to improve such models, especially by using more accurate individual flight parameters or accounting for the influence of $N1\%$ in the noise levels. This recommendation is especially intended for more sophisticated purposes, such as noise abatement studies, rather than studies on the average exposure noise levels over long time periods, where errors in the model estimates can balance out.

Additional work with other aircraft types is encouraged, especially when using signals containing a larger frequency range (i.e., no undersampled as here). Moreover, repeating this study using other noise metrics, such as EPNL or new psychoacoustic annoyance metrics [28], is of high interest. Other researchers are encouraged to apply the proposed method to calculate $N1\%$ described here to similar datasets in order to confirm the conclusions obtained in this paper.

Acknowledgments

The authors thank Dr. Michael Arntzen from Amsterdam Airport Schiphol for providing the experimental data and critical thinking preparing this paper. The authors also acknowledge Henk Veerbeek from the Netherlands Aerospace Centre (NLR) for providing data about the engines.

[1] "Global Market Forecast – Flying by Numbers 2015–2034," Tech. rep., Airbus S.A.S. Blagnac, France., 2015.

[2] "CEAC Doc. 29. Report on Standard Method of Computing Noise Contours around Civil Airports. Volume 2: Technical Guide," Tech. rep., European Civil Aviation Conference (ECAC), 2016, 4^{th} edition.

[3] Merino-Martinez, R., Bertsch, L., Snellen, M., and Simons, D. G., "Analysis of landing gear noise during approach," 22^{nd} *AIAA/CEAS Aeroacoustics Conference. May 30 – June 1 2016. Lyon, France*, 2016, AIAA paper 2016–2769.

[4] Zellmann, C., Schäffer, B., Wunderli, J. M., Isermann, U., and Paschereit, C. O., "Aircraft Noise Emission Model Accounting for Aircraft Flight Parameters," *Journal of Aircraft*, 2017.

[5] Kontos, K. B., Janardan, B. A., and Gliebe, P. R., "Improved NASA–ANOPP Noise Prediction Computer Code for Advanced Subsonic Propulsion Systems. Volume 1: ANOPP Evaluation and Fan Noise Model," Tech. Rep. NASA CR–195480, NASA CR–195480, 1996.

[6] Bertsch, L., Dobrzynski, W., and Guérin, S., "Tool Development for Low–Noise Aircraft Design," *Journal of Aircraft*, Vol. 47, No. 2, March–April 2010, pp. 694–699.

[7] Isermann, U., Matschat, K., and Mueller, E. A., "Prediction of Aircraft Noise Around Airports by a Simulation Procedure," *International Congress and Exposition of Noise Control Engineering, 21–23 July, 1986, Cambridge, Massachusetts, USA*, 1986.

[8] "Procedure for the Calculation of Airplane Noise in the Vicinity of Airports, Aerospace Information Report AIR 1845," Tech. rep., Society of Automotive Engineers, Inc. (SAE) - Committee on Aircraft Noise (SAE A-21), 400 Commonwealth Drive, Warrendale, PA 15096, January 1986.

[9] "Recommended method for computing noise contours around airports (ICAO Circular 205–AN/1/25)," Tech. rep., International Civil Aviation Organization (ICAO), Montreal, Canada., 1988.

[10] He, B., Dinges, E., Hemann, J., Rickel, D., Mirsky, L., Roof, C., Boeker, E., Gerbi, P., and Senzig, D., "Integrated Noise Model (INM) Version 7.0 User's Guide," Tech. rep., Federal Aviation Administration (FAA) – U.S. Department of Transportation, Washington, DC, April 2007, Report No. FAA-AEE-07-04.

[11] Boeker, E., Dinges, E., He, B., Fleming, G., Roof, C., Gerbi, P., Rapoza, A., and Hemann, J., "Integrated Noise Model (INM) Version 7.0 User's Guide," Tech. rep., Federal Aviation Administration (FAA) – U.S. Department of Transportation, Washington, DC, April 2008, Report No. FAA-AEE-08-01.

[12] Bergmans, D., Arntzen, M., and Lammen, W., "Noise attenuation in varying atmospheric conditions," Tech. Rep. NLR–TP–2011–262, National Aerospace Laboratory (NLR), Anthony Fokkerweg 2, 1059 CM Amsterdam, P.O. Box 90502, 1006 BM Amsterdam, The Netherlands, November 2011.

[13] Simons, D. G., Snellen, M., Midden, B., Arntzen, M., and Bergmans, D. H. T., "Assessment of noise level variations of aircraft fly–overs using acoustic arrays," *Journal of Aircraft*, Vol. 52, No. 5, September–October 2015, pp. 1625–1633.

[14] Snellen, M., Merino-Martinez, R., and Simons, D. G., "Assessment of aircraft noise sources variability using an acoustic camera," 5^{th} *CEAS Air & Space Conference. Challenges in European Aerospace. September 7 – 11 2015, Delft, Netherlands*, 2015.

[15] Snellen, M., Merino-Martinez, R., and Simons, D. G., "Assessment of noise level variability on landing aircraft using a phased microphone array," *Journal of Aircraft*, Vol. 54, No. 6, 2017, pp. 2173–2183.

[16] Merino-Martinez, R., Snellen, M., and Simons, D. G., "Determination of Aircraft Noise Variability Using an Acoustic Camera," 23^{rd} *International Congress on Sound and Vibration, July 10 – 14 2016, Athens, Greece*, 2016.

[17] Aircraft Noise and Performance (ANP) database website, "http://www.aircraftnoisemodel.org," Accessed in June 2017.

[18] Merino-Martinez, R., Snellen, M., and Simons, D. G., "Functional beamforming applied to imaging of flyover noise on landing aircraft," *Journal of Aircraft*, Vol. 53, No. 6, November–December 2016,

pp. 1830–1843.

[19] Merino-Martinez, R., Snellen, M., and Simons, D. G., "Functional Beamforming Applied to Full Scale Landing Aircraft," 6^{th} *Berlin Beamforming Conference, February 29 – March 1 2016, Berlin, Germany*, GFaI, e.V., Berlin, 2016, BeBeC–2016–D12.

[20] Merino-Martinez, R., Neri, E., Snellen, M., Kennedy, J., Simons, D., and Bennett, G., "Comparing fly-over noise measurements to full–scale nose landing gear wind–tunnel experiments for regional aircraft," 23^{rd} *AIAA/CEAS Aeroacoustics Conference. June 5 – 9 2017. Denver, Colorado, USA*, 2017, AIAA paper 2017–3006.

[21] Brüel & Kjær Airport Noise Monitoring and Management System website, "https://www.bksv.com/en/products/environment-management/airport-environment-monitoring/ANOMS," Accessed in June 2017.

[22] Schiphol Amsterdam Airport NOMOS website, "https://noiselab.casper.aero/ams/," Accessed in March 2017.

[23] Arntzen, M., *Aircraft noise calculation and synthesis in a non–standard atmosphere*, Ph.D. thesis, Delft University of Technology, 2014, ISBN: 978–94–62594–64–7.

[24] European Aviation Safety Agency (EASA) website, "http://www.easa.europa.eu," Accessed in August 2013.

[25] Royal Netherlands Meteorological Institute (KNMI) website, "http://www.knmi.nl/klimatologie/uurgegevens/," Accessed in August 2013.

[26] Lawson, C. L. and Hanson, R. J., *Solving least squares problems*, Englewood Cliffs, New Jersey, 1974, ISBN: 0–89871–356–0.

[27] Schlüter, S. and Becker, S., "Determination of aircraft engine speed based on acoustic measurements," 45^{th} *International Congress and Exposition of Noise Control Engineering, 21–24 August, 2016, Hamburg, Germany*, 2016.

[28] Sahai, A. K. and Stumpf, E., "Incorporating and Minimizing Aircraft Noise Annoyance during Conceptual Aircraft Design," 20^{th} *AIAA/CEAS Aeroacoustics Conference, June 16 – 20 2014, Atlanta, GA, USA*, 2014, AIAA paper 2014–2078.